Journal of Statistical Physics, Vol. 64, Nos. 1/2, 1991

Infinite-Range Mean-Field Percolation: Transfer Matrix Study of Longitudinal Correlation Length

V. Privman[1] and L. S. Schulman[1]

Received November 29, 1990; final February 18, 1991

Two infinite-range directed percolation models, equivalent also to epidemic models, are considered for a finite population (finite number of sites) N at each "time" (directed axis) step. The general features of the transfer matrix spectrum (evolution operator spectrum for the epidemic) are studied numerically, and compared with analytical predictions in the limit $N = \infty$. One of the models is devised to allow numerical results to be obtained for N as high as nearly 800 for the largest longitudinal percolation correlation length (relaxation time for epidemic). The finite-N behavior of this correlation length is studied in detail, including scaling near the percolation transition, exponential divergence (with N) above the percolation transition, as well as other noncritical and critical-point properties.

KEY WORDS: Finite systems; scaling; asymptotic degeneracy.

1. INTRODUCTION

The transfer matrix method, reviewed in refs. 1 and 2, has proved a powerful tool for studying thermodynamic properties of two-dimensional and in few cases, three- and higher-dimensional models. Directed percolation and related cellular automata-type systems were studied by the transfer matrix techniques mostly in the critical region.[3–8] Recently, however, there has been interest in global features of the spectrum.[8,9] Specifically, for $p > p_c$, the behavior of the correlation length associated with the leading spectral gap has been found to yield useful information, similar to the earlier studies of the Ising-model correlations[10–13] for $T < T_c$.

[1] Department of Physics, Clarkson University, Potsdam, New York 13699-5820.

822/64/1-2-14

Attempts to apply the transfer matrix method to study higher-dimensional systems have required large-scale computations and involved a combination of transfer matrix and Monte Carlo techniques.[1,2,14,15] A class of one-dimensional models with long-range interactions also allows a transfer-matrix approach,[16–18] either analytical[16] or numerical.[17,18] All these studies were limited to Ising models. Finally, in ref. 17, Ising models with infinite-range interactions *within each cross section* of the cylinder, $L^{d-1} \times \infty$, were introduced. Such models have effectively no spatial geometry or dimensionality. Their "geometry" is defined instead by the number of spins N in the cross section, with, effectively, $N \propto L^{d-1}$. The $N \times \infty$ system is thus treated by the transfer matrix method. The study of ref. 17 was focused on the analytical properties of the eigenvalues relevant to metastable states.

In this work we consider infinite-connectivity (in the cross section) $N \times \infty$ directed percolation models, following earlier studies of such models in the $N = \infty$ limit[19] in which, in fact, both the Ising and the directed percolation critical behavior are mean-field. However, our study here is not restricted to the vicinity of the critical point. Our main objective is, in fact, to investigate the large-N asymptotic behavior of the leading longitudinal correlation length.

In Section 2, we study the global features of the transfer matrix eigenvalue spectrum for a standard infinite-connectivity percolation model. In Section 3, a new modified "single-step" model is defined which has global spectral features similar to those of the model of Section 2. However, as detailed in Section 4, this new model has advantages in numerical studies of the correlation length associated with the leading spectral gap. Numerical results on the behavior of this correlation length below the percolation transition are presented in Section 5. Above the transition, the asymptotic degeneracy of eigenvalues, yielding a diverging length scale, is encountered. Detailed numerical studies of the correlation length in this regime are reported in Section 6. Section 7 is devoted to the scaling analysis in the critical region. Asymptotics of the scaling function, as well as some results on corrections to scaling, are obtained as well.

2. INFINITE-CONNECTIVITY DIRECTED PERCOLATION

In addition to the usual percolation models of the propagation of "wetness" or connectivity, there are large classes of cellular automata,[5,6] reaction-kinetics models,[20] and epidemic processes[21] which belong to the universality class of directed percolation. We will use the "epidemic" nomenclature, and furthermore, we denote the directed axis as the time axis. Thus, the longitudinal correlation lengths can be identified as relaxa-

tion times, and the transfer matrix is effectively an evolution operator of the (discrete in time and space) stochastic dynamics of the epidemic process.

In this section we consider the most straightforward definition of infinite-connectivity directed percolation[19] and describe some global features of the transfer matrix spectrum. For detailed numerical studies, however, the model will be modified: see Section 3. Here we assume that a population of N individuals consists at time t of $n(t)$ sick and $N-n(t)$ healthy members. During the time step $\Delta t = 1$, each sick individual passes the infection to the fraction p of all the population (including a possible "self-reinfection"). The multiplicity of the resulting infection (including the self-infection) does not matter: the only possible final state is "sick" or "healthy." In ref. 19, the disease associated with this epidemic was termed "percolitis."

The model has an obvious infinite-range directed percolation interpretation: each one of the N sites at time t is connected by bonds to all the N sites at time $t+1$. The bonds are open with probability p, and the "wetness" spreads along the open bonds from the $n(t)$ wet sites at time t to the $n(t+1)$ sites at time $t+1$. In order to have a nontrivial model, the probability p must be of order $1/N$. We take

$$p = \frac{x}{N} \tag{2.1}$$

and consider the limit of large N, with x of order 1.

The transition probability from the state $n(t)=j$ to the state $n(t+1)=k$ is given by

$$\text{Prob}(j \to k) = \binom{N}{k} \left[1 - \left(1 - \frac{x}{N} \right)^j \right]^k \left(1 - \frac{x}{N} \right)^{j(N-k)} \tag{2.2}$$

where the factors in (2.2) are obvious: the combinatorial coefficient corresponds to selection of which k members of the group are sick at $t+1$. The factors $[1-(1-p)^j]$ for each of those k members give the probability weight that at least one of the j sick (at t) members will indeed infect the selected "victim." Finally, the factors $(1-p)^j$ give the probability that the remaining $N-k$ group members will be healthy at time $t+1$.

The transfer matrix (evolution operator) W is defined by the matrix elements

$$W_{k,j} = \text{Prob}(j \to k) \tag{2.3}$$

which corresponds to representing the probability distribution for having n infected members as a column vector with entries labeled by

$n = 0, 1, 2, ..., N$. It is clear that W is a nonsymmetric, stochastic matrix, $\sum_{k=0}^{N} W_{k,j} = 1$ for all j.

The bulk ($N \equiv \infty$) longitudinal length scales (for percolation) or relaxation times (for the epidemic picture) can be obtained by considering the mean-field evolution equation for this model (which is exact[19] for $N = \infty$, i.e., the model is exactly mean-field in its bulk properties).

While there are several ways to derive the mean-field evolution equation, the simplest approach is to assume that at time t the most probable density is

$$\rho(t) \equiv \frac{\langle n(t) \rangle}{N} \tag{2.4}$$

where the angles denote averages, and to calculate $\rho(t+1)$ via the maximal transition probability for $n(t) \to n(t+1)$. This is appropriate only if fluctuations can be neglected. The equation

$$\frac{\partial \ln W_{\rho(t+1)N, \rho(t)N}}{\partial \rho(t+1)} = 0 \tag{2.5}$$

can be reduced, after some algebra, to

$$\ln \frac{(1-\rho)(1-R)}{\rho R} = \frac{1-2\rho}{2\rho(1-\rho)\,N} + O\left(\frac{1}{N^2}\right) \tag{2.6}$$

where $\rho \equiv \rho(t+1)$, and

$$R \equiv \left(1 - \frac{x}{N}\right)^{\rho(t)N} \simeq e^{-x\rho(t)} \tag{2.7}$$

For large N, the evolution equation is thus

$$\rho(t+1) = 1 - e^{-x\rho(t)} \tag{2.8}$$

The evolution equation (2.8) has a critical point at $x = 1$. Indeed, for $x \leqslant 1$, any initial value $0 \leqslant \rho(0) \leqslant 1$ iterates to zero. There is "no percolation" (no persistent epidemic) for $x \leqslant 1$. However, for $x > 1$, any nonzero initial density $\rho(0) > 0$ iterates to the equilibrium value $\bar{\rho}$, where $\bar{\rho}$ is in (0, 1) and satisfies the equation

$$\bar{\rho} = 1 - e^{-x\bar{\rho}} \tag{2.9}$$

Let us first consider the case $x < 1$. One can easily check that the convergence of $\rho(t)$ to zero can be expanded in an asymptotic series

$$\rho(t) \approx z_1 x^t + z_2 x^{2t} + \cdots \tag{2.10}$$

where the coefficients z_j are certain functions of the initial value $\rho(0)$ and of x, but not of t. Thus, the relaxation times ξ_m or the longitudinal correlation lengths, in the limit $N=\infty$, must correspond to $x^{mt}=\exp(-t/\xi_m)$, i.e., to

$$\xi_m(N=\infty)=-\frac{1}{m\ln x} \tag{2.11}$$

Numerical studies of the spectrum of the transfer matrix W for $N\leqslant 50$ and $0<x<3$ found no degenerate eigenvalues. Our results also suggest that as N increases, an increasing number of the largest eigenvalues are real. Note that for lower-dimensional, non-mean-field percolation problems[7,8] some eigenvalues are also complex pairs, but usually a large number of the largest eigenvalues are real, nondegenerate. The eigenvalues of the transfer matrix thus will be labeled $\Lambda_0>|\Lambda_1|\geqslant|\Lambda_2|\geqslant\ldots$. Note that $\Lambda_0\equiv 1$ here, due to the stochastic property of the transfer matrix. This corresponds (for all x) to the trivial value $\xi_0=\infty$, corresponding, in turn, to a possible evolution with no sick group members, $n(t)\equiv 0$, which is an "absorbing state" in the stochastic processes nomenclature.

For $0<x<1$, we found that the eigenvalues approach the limiting (large N) values suggested by the general relation

$$\xi_i(x,N)\equiv\frac{\Delta t}{\ln(\Lambda_0/\Lambda_i)}=-\frac{1}{\ln\Lambda_i} \tag{2.12}$$

Indeed, numerical evidence suggests that

$$\Lambda_m(x<1,N)\to x^m \qquad \text{as} \qquad N\to\infty \tag{2.13}$$

as illustrated in Fig. 1.

Consider now the case $x>1$. It turns out that there is a kind of a *duality* property in the percolation problem at hand. Let us define the quantities

$$\tilde{x}=x(1-\bar{\rho}) \qquad \text{and} \qquad \tilde{\rho}(t)=\frac{\rho(t)-\bar{\rho}}{1-\bar{\rho}} \tag{2.14}$$

One can show by a straightforward algebra that for $1<x<\infty$ the tilde-marked new quantities satisfy the same relations as the original x and ρ for $0<x<1$. Specifically, $\tilde{x}<1$, and (2.8) applies for $\tilde{\rho}$, provided $\tilde{x}$ is used in place of x. Thus, the equivalent of (2.13) would be the conclusion that the eigenvalues of the transfer matrix for $x>1$ are powers of $\tilde{x}$.

However, numerical studies indicate an interesting "finite-size" feature:

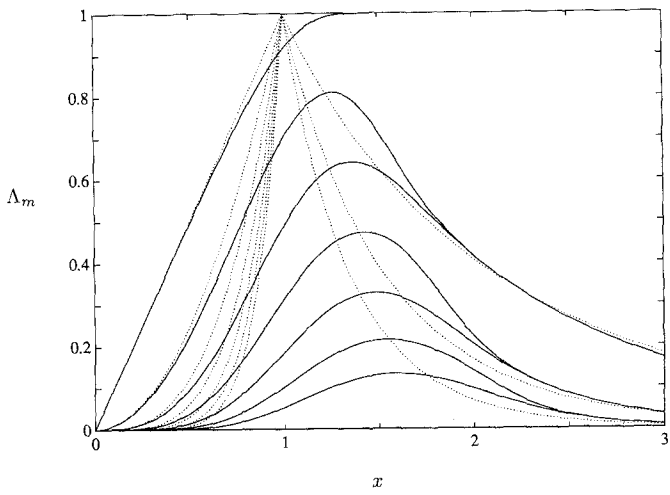

Fig. 1. Solid curves: The seven largest nontrivial eigenvalues $\Lambda_1, ..., \Lambda_7$ for the infinite-range percolation model defined in Section 2. The values shown were obtained numerically for $N = 30$. Dotted curves: The theoretical limiting values: x, $x^2, ..., x^7$ for $x < 1$, and $\tilde{x}$, $\tilde{x}^2$, $\tilde{x}^3$ for $x > 1$, see text.

the eigenvalues actually approach $\tilde{x}^m$ in pairs; see Fig. 1. Thus, $\Lambda_1 \to 1$ (and $\Lambda_0 \equiv 1$); $\Lambda_{2,3} \to \tilde{x}$; $\Lambda_{4,5} \to \tilde{x}^2$; etc. The asymptotic degeneracy (exponentially small-in-N gap) of the largest nontrivial eigenvalue Λ_1 with Λ_0 is a general feature of directed percolation models,[9] shared with Ising[10–13] and isotropic percolation models.[22,23] The degeneracy of the higher-order eigenvalues is probably special to the mean-field percolation.

As indicated in the introduction, the objective of our study is to investigate in detail the behavior of the leading eigenvalue gap, and the associated correlation length $\xi_{||} = \xi_1$. Indeed, this length is finite below the critical-point value $x = 1$; it diverges exponentially for x above 1; and in fact it diverges algebraically, as do other correlation lengths (all gaps close up) at $x = 1$: see Fig. 1. However, the infinite-range percolation model just studied allows only some qualitative conclusions to be made from numerical studies (such as Fig. 1). The reason for numerical difficulties lies in the fact that the matrix elements (2.3) are strongly varying in magnitude. Thus, roundoff errors plague numerical routines. On the other hand, it turns out (see Sections 5–7) that the system sizes N needed to observe various asymptotic behaviors are quite large. Thus, in the next section we will introduce a new mean-field infinite-connectivity directed percolation model which will be used in the numerical studies reported in Sections 4–7.

3. SINGLE-STEP PERCOLATION MODEL

To construct a model that will be easier to handle numerically, we will further discretize the time evolution. We define a model in which the time steps are much less than 1, and in which at most one disease transmission can occur during each time step. Let there be n sick members at time t. One group member is randomly selected and termed "active." If this "active" member is healthy, then nothing happens. However, if the "active" member is sick (probability n/N), then we assume that it can be cured at that time step, corresponding to $n \to n-1$, or that it can infect one additional group member out of the initially $N-n$ healthy subgroup. The latter process corresponds to $n \to n+1$ and its probability is proportional to $(N-n)/N$. Both the rates of "cure" and "infection" must be of order $1/N$, due to the infinite connectivity in the cross section, to have the analogy with the model of Section 2. Instead of tabulating all possible outcomes with their probabilities, we will simply assign weight factors $1/N$ for cure and x/N for infection. (Various detailed selection rules may differ by terms of order $1/N$.) Thus, we take the transition probabilities in the form

$$\text{Prob}(n \to n-1) = \frac{n}{N} \times \frac{1}{N} = \frac{n}{N^2} \tag{3.1}$$

$$\text{Prob}(n \to n+1) = \frac{n}{N} \times \frac{N-n}{N-1} \times \frac{x}{N} = \frac{n(N-n)\,x}{N^2(N-1)} \tag{3.2}$$

$$\begin{aligned} \text{Prob}(n \to n) &= 1 - \text{Prob}(n \to n-1) - \text{Prob}(n \to n+1) \\ &= 1 - \frac{n}{N^2}\left[1 + \frac{(N-n)\,x}{N-1}\right] \end{aligned} \tag{3.3}$$

No other transitions are allowed.

The overall rate of, e.g., cure per sick member must be of order 1 for time steps of order 1, while our rate in (3.1) is proportional to $1/N^2$. In order to establish a correspondence with the model of Section 2, we must thus take the time steps here to be of order $1/N^2$. Since we have already absorbed an arbitrary factor in the rates by fixing the cure rate $\propto 1$, as opposed to the infection rate $\propto x$, we can put

$$\Delta t \equiv \frac{1}{N^2} \tag{3.4}$$

without any loss of generality. The model proposed here will then not be identical, but may be expected to be "universal," with the model of Section 2.

The transfer matrix T for this new "single-step" model is constructed from the transition probabilities (3.1)–(3.3) in an obvious manner. It is a tridiagonal, stochastic matrix. Let us denote its eigenvalues by $\lambda_0 > |\lambda_1| \geqslant |\lambda_2| \geqslant \ldots$. Our numerical studies of the global features of the spectrum up to $N = 50$, with $0 < x < 4$, indicate that an increasing (with N) number of the largest eigenvalues are real, and there are no degeneracies. Here, as before, we have $\lambda_0 \equiv 1$. However, a "global" comparison with the model of Section 2 is simpler if we consider the eigenvalues of the matrix $W = T^{N^2}$, which corresponds to $\Delta t = 1$. Thus, we denote $\Lambda_m = \lambda_m^{N^2}$ for the single-step model.

The mean-field evolution equation for the single-step model is no longer of the recursive type (2.8). Indeed, the difference $[\rho(t+\Delta t) - \rho(t)]$ is of order $1/N^2$. For large N, it will be replaced by $\Delta t\, d\rho/dt$. The Ω-expansion technique[24] provides a systematic method to derive the mean-field evolution equation. Only the result is given here:

$$\frac{d\rho}{dt} = \rho(x - 1 - x\rho), \qquad \text{where} \quad \rho \equiv \rho(t) \tag{3.5}$$

The critical point is at $x = 1$. For $x \leqslant 1$, $\rho(t)$ decays to zero for any initial value $0 \leqslant \rho(0) \leqslant 1$. However, for $x > 1$ any nonzero initial value evolves (as $t \to \infty$) to the steady-state density

$$\bar{\rho} = \frac{x-1}{x} \tag{3.6}$$

For $x < 1$, examination of the differential equation (3.5) immediately suggests that the relaxation times are [compare (2.11)]

$$\xi_m(N = \infty) = \frac{1}{m(1-x)} \tag{3.7}$$

Numerical studies indicate (see Fig. 2) that the eigenvalues Λ_m converge to the limiting values [compare (2.13)],

$$\Lambda_m(x < 1, N) \to \exp[-m(1-x)] \qquad \text{as} \quad N \to \infty \tag{3.8}$$

with a one-to-one correspondence.

For $x > 1$ there is no longer an exact duality-type transformation. However, the difference

$$\tilde{\rho}(t) \equiv \rho(t) - \bar{\rho} \tag{3.9}$$

satisfies the equation

$$\frac{d\tilde{\rho}}{dt} = \tilde{\rho}(1 - x - x\tilde{\rho}) \tag{3.10}$$

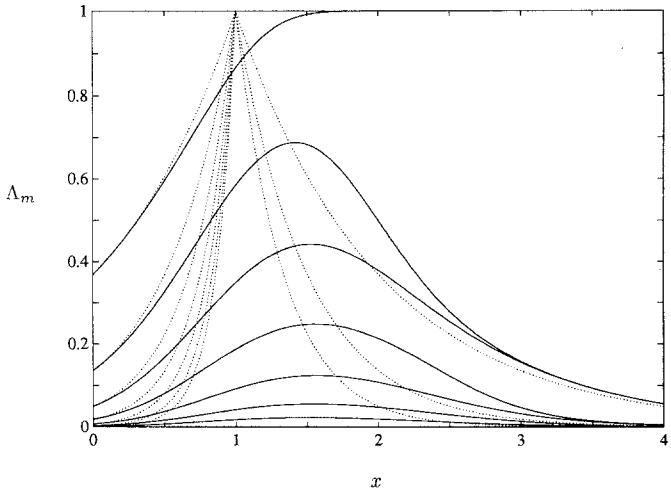

Fig. 2. Solid curves: The seven largest nontrivial eigenvalues $\Lambda_1, ..., \Lambda_7$ for the single-step percolation model defined in Section 3. The values shown were obtained numerically for $N = 50$. Recall that Λ_m are related to the actually calculated eigenvalues λ_m via $\Lambda_m = \lambda_m^{N^2}$. Dotted curves: The theoretical limiting values: $\exp[m(x-1)]$, $m = 1, 2, ..., 7$, for $x < 1$, and $\exp[m(1-x)]$, $m = 1, 2, 3$, for $x > 1$; see text.

This is quite similar to (3.5). Numerical studies, such as Fig. 2, indicate that here again we have the spectrum-doubling feature: the "bulk" correlation lengths (relaxation times) are $1/[m(x-1)]$, but they correspond to pairs of the finite-N eigenvalues. Thus, we have $\Lambda_1 \to 1$ (and $\Lambda_0 \equiv 1$); $\Lambda_{2,3} \to \exp(1-x)$; $\Lambda_{4,5} \to \exp[2(1-x)]$; etc. Figure 2 further illustrates the global features of the leading eigenvalues.

4. NUMERICAL CALCULATION OF THE LEADING EIGENVALUE

In order to study numerically the details of the finite-N behavior, we consider the single-step model defined in Section 3 and focus our attention on the largest nontrivial eigenvalue λ_1. The reasons for considering the leading eigenvalue are first due to the fact that the largest correlation length has interesting properties for $x > 1$ associated with the asymptotic degeneracy with $\lambda_0 = 1$. This feature is quite general and is also found in non-mean-field percolation models.[9,22,23] Second, an efficient numerical evaluation of this leading eigenvalue is possible.

We define the reduced, $N \times N$, transfer matrix U to be the same as T except that it lacks the $n = 0$ row and column. Since the state $n = 0$ is "absorbing," the matrix U thus has only the eigenvalues $\lambda_1, ..., \lambda_N$. An

interesting feature of the single-step model is that all its leading eigenvalues are quite close to 1, for all $0 < x < \infty$. Indeed, we argued in Section 3 that an unbounded number of the largest eigenvalues of $W = T^{N^2}$, denoted by Λ_m, eventually approach limiting values in $(0, 1]$ (for $0 < x < \infty$). However, λ_m are given by Λ_m^{1/N^2}. Thus, the differences $(1 - \lambda_m)$ are at least as small as const$/N^2$.

Our numerical procedure for estimating λ_1 was based on the iteration method. The estimate $u_{(j)}$ of the eigenvector of U belonging to λ_1 was refined by calculating $u_{(j+1)}$ by solving the linear equation

$$(1 - U)\, u_{(j+1)} = u_{(j)} \tag{4.1}$$

Such methods are standard in numerical analysis, and details can be found in the literature; see, e.g., ref. 25. Specifically, we used the Crout reduction algorithm for the solution of the tridiagonal linear system (4.1).

This numerical procedure is extremely efficient for the model at hand, due to the proximity of λ_1 to 1. For increasing N, the numerical convergence (at fixed x) is limited by the roundoff errors. The maximal value of N, denoted $N_{\max}(x)$, reachable for $x = 0.01, 0.02, \ldots, 3.00$, without having roundoff convergence problems (required accuracy in λ_1 was of order 10^{-14}), is given in Fig. 3. Note that the values in Fig. 3 do not vary smoothly. In fact, $N_{\max}(x)$ is computer-dependent. We tried three different computers, and the best results were obtained on the SUN-3/280 workstation (with FPA board). All our calculations, and the values in Fig. 3, were based on the SUN-workstation runs, in the standard double-precision Fortran. As emphasized, the numerical procedure is extremely efficient, and CPU time was not at all a limiting factor.

The basic quantity that we consider is

$$\xi_{||}(x, N) \equiv \xi_1 \equiv \frac{\Delta t}{\ln(\lambda_0/\lambda_1)} = -\frac{1}{N^2 \ln \lambda_1} \tag{4.2}$$

As suggested by the data in Fig. 3, for x approximately in the range 0.5–1.5, which includes the critical point at 1, we can obtain $\xi_{||}$ accurately for N values as high as 400, up to nearly 800 for some x values. For example, $N_{\max}(x = 1) = 648$. The convergence gets worse for very small x values, and also for x larger than 2. Fortunately, however, the x range for which large-N results are obtainable includes all the typical regimes: $x < 1$, x near 1, and $x > 1$.

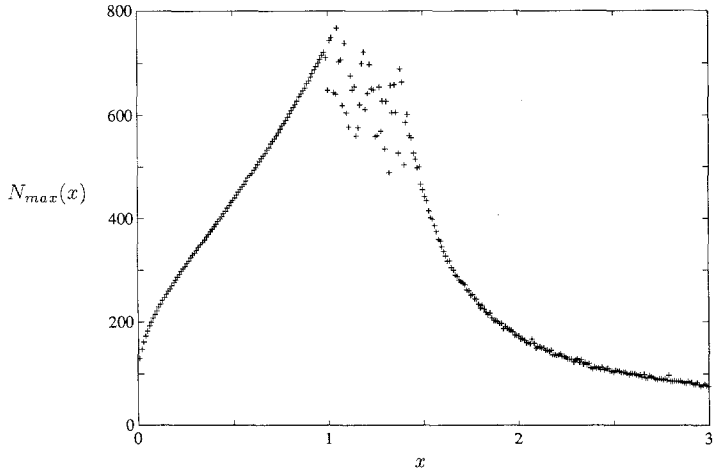

Fig. 3. The values of N reachable in numerical calculations for fixed x, denoted by $N_{\max}(x)$; see Section 4.

5. CORRELATION LENGTH BELOW THE PERCOLATION TRANSITION

For fixed $0 < x < 1$, we expect the correlation length to converge to its bulk limiting value; see (3.7) with $m = 1$. In this section we summarize the numerical evidence indicating that this convergence is in inverse powers of N,

$$\xi_{||}(x, N) = \frac{1}{1-x} + \frac{B(x)}{N} + \frac{B^{(2)}(x)}{N^2} + \cdots \tag{5.1}$$

Little is known in the literature about "noncritical" finite-size corrections for infinite-range models. For the Ising and related lattice-gas models of $\mathcal{N}$ spins (particles) interacting with each other via ferromagnatic coupling of order $1/\mathcal{N}$, it has been argued[11,26] that the corrections to the thermodynamic properties are indeed in powers of $1/\mathcal{N}$. We are not aware of any results for correlation properties. The $1/N$ correction here, and also the $1/\mathcal{N}$ correction in the fully finite model case just mentioned, are naturally associated with the fact that changes in system properties when the size is changed from N to $N + O(1)$ will "follow the extensivity," i.e., they will be of *relative* magnitude N^{-1} (or $\mathcal{N}^{-1}$).

The competing types of correction that one could think of are the Gaussian, order $1/\sqrt{N}$ (or $1/\sqrt{\mathcal{N}}$) fluctuations. However, these only show up near criticality,[27] where the "extensivity" of various quantities loses its meaning due precisely to large fluctuations; see Section 7 below.

We considered the $\xi_{||}$ data for $x = 0.4$, 0.5, 0.6, 0.7, 0.8. The $N_{\max}(x)$ values were 384, 435, 487, 544, 603, respectively. The N dependence for each x was fit by using 10-, 20-, and 40-point least-squares fits to the two-, three-, four-, and five-term representation (5.1), with the points for the fit selected as N_0, $N_0 - 1$, ..., where N_0 took values from $N_{\max}$ down to $N_{\max} - 100$. Only the two- and three-term fits gave stable results. The higher-number-of-terms [in (5.1)] fits were less stable due to the roundoff noise in the data. The quality (consistency) of the stable fits was measured by the rms deviation.

For $x = 0.4$, 0.5, 0.6, the rms deviation was typically of order 10^{-10}, which exceeded the consistency of similar fits assuming, e.g., a series in powers of $1/\sqrt{N}$ instead of $1/N$. However, for $x = 0.8$ and, to a lesser extent, for $x = 0.7$, the linear-power fits were no longer clearly favored. We interpret this as an indication of the proximity of the critical region, which is very wide for this model (see Section 7 below). It is expected that the asymptotic behavior (5.1) will set in for larger N values, for x near 1. In fact, as $x \to 1$, the N values needed diverge as $\sim (1-x)^{-2}$ (as follows from the results of the later sections), while our $N_{\max}(x)$ are bounded near $x = 1$.

The consistency of the form (5.1) was also confirmed by the exact fitting of the two- and three-term representation (5.1) to the values $\xi_{||}(x, N_0 + 1 - k)$, $k = 1, 2$ or $k = 1, 2, 3$, respectively. As with the least squares, higher-term fits were less stable due to roundoff noise. The stability was checked by considering the variation with N_0.

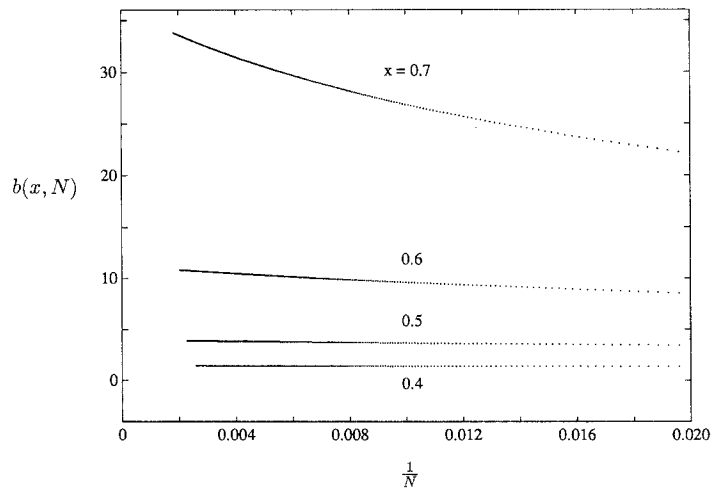

Fig. 4. The estimators $b(x, N)$ defined in (5.2), vs. $1/N$, for the x values 0.4 (the bottom set), 0.5, 0.6, and 0.7 (the topmost set).

In order to illustrate the linearity in $1/N$, we present in Fig. 4 the estimated $b(x, N)$, of $B(x)$, vs. $1/N$, where we define

$$b(x, N) = N\left[\frac{1}{1-x} - \xi_{||}(x, N)\right] \tag{5.2}$$

These quantities show a clear linear variation [due to the $B^{(2)}$ correction in (5.1)] for $x = 0.4$, 0.5, 0.6, and, to a lesser extent, for $x = 0.7$.

6. ASYMPTOTIC DEGENERACY ABOVE THE PERCOLATION TRANSITION

Asymptotic degeneracy of the two largest transfer matrix eigenvalues has long been a topic of fascination and study, dating at least as far back as Onsager's solution of the two-dimensional Ising model.[28] Surprisingly, however, most of the results available to date[10–14,16,28] have been for Ising models: asymptotic degeneracy has been linked to the buildup of the first-order phase transitions, to interfacial fluctuations, to hyperscaling properties on approach to criticality, etc. Results for n-vector models were reported in ref. 29. Recently, a study of the leading transfer matrix spectral gap was reported for the $(1+1)$-dimensional Reggeon field theory, universal with two-dimensional directed percolation.[9]

The length scale $\xi_{||}$ measures, for $x > 1$, the persistence of the epidemic; $\xi_{||}$ is very large above the percolation threshold. Indeed, for $N = \infty$, the epidemic would persist indefinitely. However, for large $N < \infty$, there is a small but finite probability of no infection propagating (no connectivity) due to the fact that the state $n = 0$ is absorbing. The probability of a "break" in connectivity must be a small number raised to the power N. Thus, we define

$$\xi_{||}(x, N) \equiv e^{\Sigma(x, N)N} \tag{6.1}$$

We expect $\Sigma(x, N)$ to have a finite limiting value $\sigma(x)$, for each fixed $x > 1$. A general pattern of finite-N corrections can be proposed,[9]

$$\Sigma(x, N) = \sigma(x) + \frac{u(x) \ln N}{N} + \frac{A(x)}{N} + \frac{A^{(2)}(x)}{N^2} + \cdots \tag{6.2}$$

Here the terms with coefficients A, $A^{(2)}$, etc., are the usual "noncritical" corrections appropriate for the infinite-range models; see Section 5, e.g., (5.1). The possible logarithmic term has been typically associated with fluctuations of the transverse interfaces in the Ising case[10–14] in which the function $u(x)$ is in fact a universal constant calculable in the capillary-wave

theory. For lower-dimensional directed percolation there is numerical evidence[9] for the logarithmic contribution. The function $u(x)$ is no longer constant, and its connection with a detailed "fluctuation" picture of a break in the directed-percolation cluster connectivity in the cross section has not been clarified.

Our numerical studies indicate that for the single-step infinite-range model, there is no such correction, i.e.,

$$u(x) \equiv 0 \tag{6.3}$$

A posteriori, this could be expected due to the general suppression of fluctuations in the mean-field case. Our numerical studies consisted of the least-squares and exact fits similar to those described in Section 5. However, the clearest evidence for the absence of the logarithmic correction was obtained by plotting the data for $x = 1.1, 1.2, 1.3$ vs. $1/N$ and, on the same plot, vs. $(\ln N)/N$. Note that the $N_{\max}$ values were 604, 611, 534 for the three x values, respectively. The data for $N \gtrsim 300$ show a clear curvature in the logarithmic case, while the $1/N$ plots look very straight. The quality of the least-squares fits to the form (6.1) without the logarithmic term was comparable to that obtained below $x = 1$, where we used (5.1).

On approach to criticality, the function $\sigma(x)$ is characterized by a critical exponent,

$$\sigma(x) \approx \text{const}(x-1)^{\mu} \tag{6.4}$$

The exponent μ for the short-range directed models below their upper critical dimensionality is given by

$$\mu = (d-1)\nu_{\perp} \qquad \text{or} \qquad \mu = (d-1)\nu_{\perp} + \zeta\nu_{\|} \tag{6.5}$$

where the first relation is the generic form, applicable also in the Ising case (with $\nu_{\perp}$ replaced by ν), based on certain hyperscaling properties; see ref. 9 for details. The second relation is based on a modified scaling picture and is more consistent with the presently available numerical data for two-dimensional directed percolation.[9] In this case ζ is the leading irrelevant-variable correction-to-scaling exponent.

However, in the mean-field limit of the dimensionality d approaching its upper critical value 5, we have $\zeta \to 0$, and also $\nu_{\perp} \to \frac{1}{2}$, $\nu_{\|} \to 1$; see, e.g., ref. 4. Since it is generally the case that the mean-field exponents can be obtained in such a limiting procedure, we expect to have

$$\mu = 2 \tag{6.6}$$

In order to verify this prediction, we obtained data for $\Sigma(x, N)$ for $x = 1.002, 1.004, \ldots, 1.300$. These data were fitted by the two- and three-term

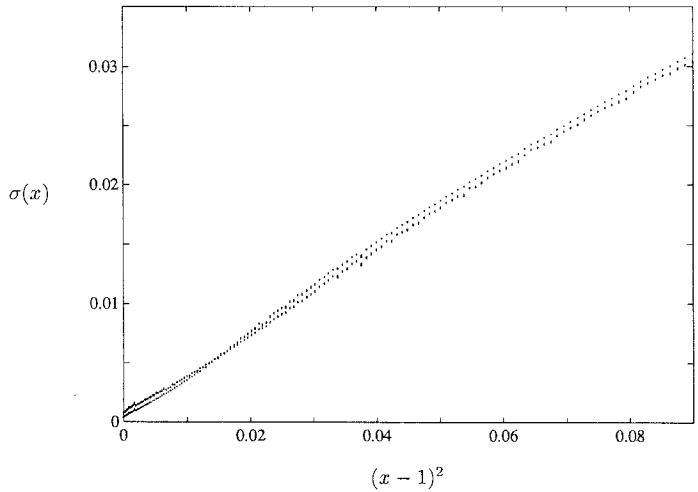

Fig. 5. The estimates of the function $\sigma(x)$ defined in Section 6, plotted vs. $(x-1)^2$. The results shown were obtained by various two- and three-term least-squares fits described in the text.

least-squares fits, with $u \equiv 0$ in (6.2). We used 20-point fits, i.e., the points N_0, $N_0 - 1$, ..., $N_0 - 19$. The resulting estimates for $\sigma(x)$ were plotted vs. $(x-1)^2$ for the choices $N_0 = N_{\max}$, $N_{\max} - 10$, ..., $N_{\max} - 60$, for each of the x values considered; see Fig. 5. Thus, for each x in Fig. 5 we have two groups of seven points each. One group are the two-term fit estimates, and another the three-term fits. The spread within each group and that between the two groups illustrate the consistency and possible systematic errors in the estimates of σ. In Fig. 5, the two-term fit results cluster lower than the three-term results, except for the smallest abscissa values, below ~ 0.015.

The exponent value $\mu = 2$ corresponds to the quadratic dependence $\sigma(x) \propto (x-1)^2$ only in the critical region, i.e., for x close to 1. However, the data in Fig. 5 are quite straight for x values up to about 1.25. Indeed, the critical region for this model is quite wide, as will be confirmed also by scaling studies near $x = 1$; see Section 7 below. The fact that for the smallest x values, below about 1.07, there are deviations from the straight-line behavior in Fig. 5 simply indicates that the N values were not large enough, a situation similar to the convergence problems discussed in Section 5.

7. SCALING ANALYSIS NEAR THE CRITICAL POINT

Analysis of the N dependence for fixed x fails for $x \simeq 1$, as the results of Sections 5 and 6 indicate. This difficulty is expected. Indeed, near the

critical point the appropriate data analysis should be based on the finite-size (finite-N) scaling form of the correlation length. Below the upper critical dimension, the scaling combination is $[(p-p_c)/p_c]\, L^{1/\nu_\perp}$, where L is the transverse system size mentioned in the introduction. As the dimensionality approaches the upper critical value 5, we take the limits $\nu_\perp \to 1/2$ and $L \propto N^{1/(d-1)} \to N^{1/4}$. Thus, the appropriate scaling combination in the mean-field theory may be expected to be $(x-1)\sqrt{N}$.

The finite-N scaling form for the correlation length is

$$\xi_{||} \simeq \sqrt{N}\, X[(x-1)\sqrt{N}] \tag{7.1}$$

The power of N outside the function X will be justified when we consider the emergence of the bulk limit for $x<1$; see below. The "scaling" interpretation of (7.1) is that the limits $x \to 1$ and $N \to \infty$ are taken simultaneously, but at such rates that the combination of variables

$$s \equiv (x-1)\sqrt{N} \tag{7.2}$$

remains of order 1.

We attempted numerical data collapse according to (7.1). For each of the x values 0.850, 0.851, ..., 1.149, 1.150, we calculated $\xi_{||}(x, N)$ for $N = N_{\max}(x)$, $N_{\max}(x)-20$, ..., $N_{\max}(x)-200$. The total of 3311 values thus obtained were plotted as $\xi_{||}/\sqrt{N}$ vs. s. The resulting data collapse was quite accurate for $-3 \lesssim s \lesssim 3$. The central part of this plot, estimating the scaling function $X(s)$, is shown in Fig. 6. The quality of the data collapse for the

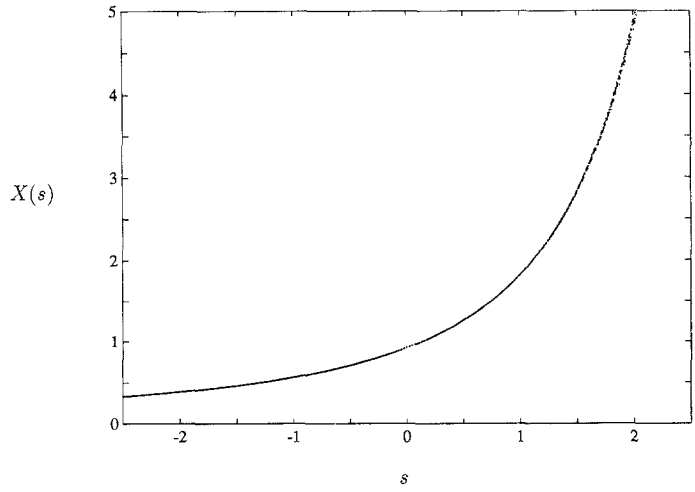

Fig. 6. The scaling data collapse. The data shown estimate the scaling function $X(s)$ defined in Section 7; see (7.1).

N values reachable in our calculations is quite sufficient to confirm the scaling form (7.1).

For larger values of $|s|$, it is interesting to examine the onset of the "bulk limit," i.e., the crossover to the fixed-x, $N \to \infty$ pattern of behavior. Let us first consider the case of large, negative s. The correct bulk limit is then obtained if we assume that

$$X(s) \approx -\frac{1}{s} \qquad \text{for} \quad s \to -\infty \tag{7.3}$$

Indeed, the bulk result $\xi_{||}(x<1, N=\infty) = 1/(1-x)$ then follows from (7.1). Numerical verification of (7.3) is presented in Fig. 7. The data here are the same as in Fig. 6, but instead of the estimates of $X(s)$, we plotted the values of $-sX(s)$. The latter function should approach 1 as $s \to -\infty$, as is indeed clearly confirmed by the data (Fig. 7).

Consider next the limit of large, positive s. In order to reproduce the bulk-limiting behavior suggested by (6.1)–(6.2) [with $u(x)=0$], one has to assume the form

$$X(s) \propto \frac{e^{\text{const } s^2}}{s} \tag{7.4}$$

as $s \to +\infty$. In order to check for this behavior, we used the same data as in calculations for Fig. 6. However, we plotted the function $\ln[sX(s)]$ vs. s^2 in Fig. 8. The expected linear behavior sets in for $s \gtrsim 2$ (see Fig. 8).

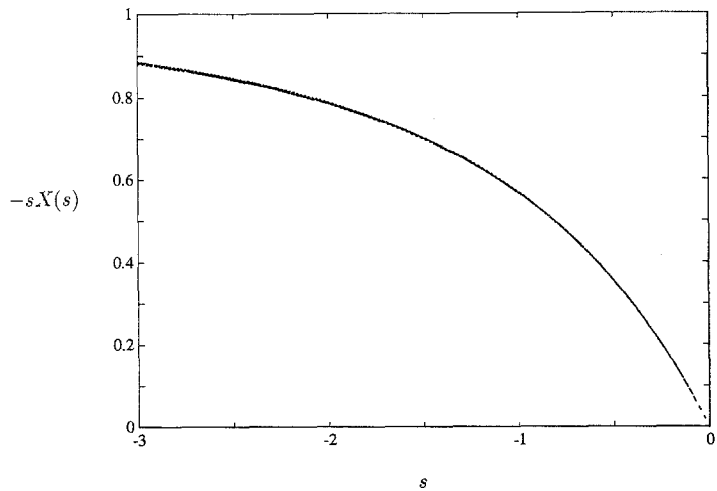

Fig. 7. Numerical estimates of $-sX(s)$ for negative s. The theoretical asymptotic limit as $s \to -\infty$ is 1.

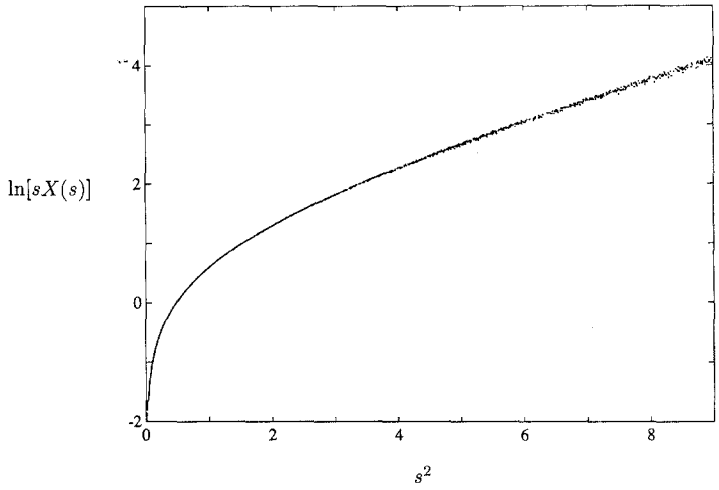

Fig. 8. Numerical estimates of $\ln[sX(s)]$, plotted vs. s^2, for positive s. The theoretical asymptotic behavior for large s^2 must be linear.

Finally, we analyzed the correction-to-scaling pattern at $s=0$, i.e., at the critical point $x=1$. Generally, the short-range mean-field models (high-dimensional models) and the infinite-range models are not necessarily "universal" at the level of corrections to scaling. This effect is due to the possibility of fluctuations away from the uniform order parameter in the short-range case as opposed to the infinite-range models. Thus, the infinite-range models have only a subset of correction contributions due to the uniform, Gaussian fluctuations. These are naturally of relative magnitude $1/\sqrt{N}$ in the critical region.[12,27]

While the full finite-N scaling-with-corrections description can be formulated, its precise verification would be difficult with the available data. Thus, we only consider the behavior at $x=x_c$. Relation (7.1) is replaced by the series

$$\xi(x=1, N)=\sqrt{N}\,X(0)+X^{(2)}+\frac{X^{(3)}}{\sqrt{N}}+\cdots \tag{7.5}$$

This representation was checked by the least-squares and exact fits similar to those described in Section 5. Our numerical estimates of the leading and the first correction amplitudes are

$$X(0)=0.9000\pm 0.0003 \qquad \text{and} \qquad X^{(2)}=0.70\pm 0.03 \tag{7.6}$$

In summary, our results reported in this work provide a qualitative picture of the global eigenvalue spectrum of the transfer matrix for the

infinite-range percolation models. Detailed numerical studies yield new information on the pattern of the finite-N behavior of noncritical properties, on the asymptotic degeneracy of the leading spectral gap, and on the scaling behavior near criticality. While some of the properties noted, such as the doubling of the subleading spectrum above the percolation transition, are probably special to infinite-range models, other results, especially those on scaling and asymptotic degeneracy, will be of use as the mean-field limits of the general-dimensionality, short-range lattice models.

ACKNOWLEDGMENTS

The authors acknowledge useful discussions with Professors D. ben-Avraham, R. Bidaux, and H. L. Frisch. This research was supported in part by the NSF via grants PHY-88-11106 and PHY-90-15858.

REFERENCES

1. M. P. Nightingale, in *Finite Size Scaling and Numerical Simulation of Statistical Systems*, V. Privman, ed. (World Scientific, Singapore, 1990), Chapter VII, p. 287.
2. M. Henkel, in *Finite Size Scaling and Numerical Simulation of Statistical Systems*, V. Privman, ed. (World Scientific, Singapore, 1990), Chapter VIII, p. 353.
3. W. Kinzel and J. M. Yeomans, *J. Phys. A* **14**:L163 (1981).
4. W. Kinzel, *Ann. Israel Phys. Soc.* **5**:425 (1983).
5. W. Kinzel, *Z. Phys. B* **58**:229 (1985).
6. L. S. Schulman and P. E. Seiden, *J. Stat. Phys.* **19**:293 (1978).
7. M. Henkel and H. J. Herrmann, *J. Phys. A* **23**:3719 (1990).
8. D. ben-Avraham, R. Bidaux, and L. S. Schulman, *Phys. Rev. A* (1991), in press.
9. M. Henkel and V. Privman, *Phys. Rev. Lett.* **65**:1777 (1990).
10. M. E. Fisher, *J. Phys. Soc. Japan Suppl.* **26**:87 (1969).
11. V. Privman and M. E. Fisher, *J. Stat. Phys.* **33**:385 (1983).
12. E. Brézin and J. Zinn-Justin, *Nucl. Phys. B* **257[FS14]**:867 (1985).
13. V. Privman and N. M. Švrakić, *J. Stat. Phys.* **54**:735 (1989).
14. K. Jansen, I. Montvay, G. Münster, T. Trappenberg, and U. Wolff, *Nucl. Phys. B* **322**:698 (1989).
15. M. A. Novotny, preprint (1990).
16. M. Kac, in *Brandeis Lectures*, M. Chretien, E. P. Gross, and S. Deser, eds. (Gordon and Breach, New York, 1968), Vol. 1, p. 241.
17. M. A. Novotny, W. Klein, and P. A. Rikvold, *Phys. Rev. B* **33**:7729 (1986).
18. Z. Glumac and K. Uzelac, *J. Phys. A* **22**:4439 (1989).
19. L. S. Schulman and P. E. Seiden, *Science* **233**:425 (1986); see also *J. Stat. Phys.* **27**:83 (1982).
20. R. Dickman, *Phys. Rev. B* **40**:7005 (1989).
21. H. K. Janssen, B. Schaub, and B. Schmittmann, *J. Phys. A* **21**:L427 (1988).
22. S. S. Manna and N. M. Švrakić, preprint (1990).
23. M. Henkel and V. Privman, *Int. J. Mod. Phys. B* (1991), in press.
24. N. G. van Kampen, *Stochastic Processes in Physics and Chemistry* (North-Holland, Amsterdam, 1981), Chapter IX.

25. R. L. Burden and J. D. Faires, *Numerical Analysis* (PWS Publishers, Boston, 1985), Section 6.7.
26. T. L. Hill, *Thermodynamics of Small Systems, Part I* (Benjamin, New York, 1963); *Part II* (Benjamin, New York, 1964).
27. V. Privman, *Physica* **123A**:428 (1984).
28. L. Onsager, *Phys. Rev.* **65**:117 (1944).
29. M. E. Fisher and V. Privman, *Phys. Rev. B* **32**:447 (1985).